Available online at www.sciencedirect.com
ScienceDirect
Journal of Nuclear Materials 373 (2008) 164–178
journal of nuclear materials
www.elsevier.com/locate/jnucmat

Corrosion behavior of steels in liquid lead–bismuth with low oxygen concentrations

Yuji Kurata *, Masatoshi Futakawa, Shigeru Saito

Japan Atomic Energy Agency, Tokai-mura, Naka-gun, Ibaraki-ken 319-1195, Japan

Received 1 August 2006; accepted 26 May 2007

Abstract

Corrosion tests in pots were conducted to elucidate corrosion behavior of various steels in liquid lead–bismuth for 3000 h under the condition of an oxygen concentration of 5×10^{-8} wt% at 450 °C and an oxygen concentration of 3×10^{-9} wt% at 550 °C, respectively. Significant corrosion was not observed at 450 °C for ferritic/martensitic steels, F82H, Mod.9Cr–1Mo steel, 410SS, 430SS except 2.25Cr–1Mo steel. Pb–Bi penetration into steels and dissolution of elements into Pb–Bi were severe at 550 °C even for ferritic/martensitic steels. Typical dissolution attack occurred for pure iron both at 550 °C without surface Fe_3O_4 and at 450 °C with a thin Fe_3O_4 film. Ferritization due to dissolution of Ni and Cr, and Pb–Bi penetration were recognized for austenitic stainless steels, 316SS and 14Cr–16Ni–2Mo steel at both temperatures of 450 °C and 550 °C. The phenomena were mitigated for 18Cr–20Ni–5Si steel. In some cases oxide films could not be a corrosion barrier in liquid lead–bismuth.

PACS: 81.65.K; 28.41.T

1. Introduction

Lead and lead–bismuth eutectic(LBE) are promising candidate materials of core coolants and high-power spallation targets of accelerator driven systems (ADSs) for transmutation of radioactive wastes and of coolants of fast reactors(FRs). However, compatibility of materials with liquid lead and LBE is one of critical issues to develop the ADSs and the FRs. In previous Russian studies [1–3], importance of oxygen control in lead and LBE was pointed out and martensitic steels containing Si were developed for corrosion resistance. It was proposed that the corrosion was characterized by dissolution of alloy components (liquid metal corrosion) at low oxygen concentrations and oxidation at middle and high oxygen concentrations [1,2]. Corrosion was mitigated for the 12 wt%Cr martensitic steel with Si addition developed in Russia under the condition of controlled oxygen concentrations for Fe_3O_4 formation [3].

The active oxygen control technique in LBE has been one of key technologies to form self-heeling protective oxides on steels and to prevent slag formation and plugging [3–5]. The oxygen concentration was controlled within the range between Fe_3O_4 formation and PbO formation. However, the lower limit of the oxygen concentration at Fe_3O_4 formation potential has not been well-grounded. Temperature and oxygen concentration dependency of the oxide films has not been clarified since experimental data are scarce under the condition near and below Fe_3O_4 formation.

Experimental studies have been performed recently for development of ADSs and FRs with a LBE coolant [6–27]. Ferritization of austenitic stainless steels due to Ni dissolution into LBE has been reported under the condition of high and middle oxygen concentrations above 550 °C [9,11,15,23,24]. The stability of oxide layers formed in LBE was studied at various temperatures and oxygen concentrations [12,18,20]. The experimental results showed

* Corresponding author. Tel.: +81 29 282 5059; fax: +81 29 282 6489.
E-mail address: kurata.yuji@jaea.go.jp (Y. Kurata).

0022-3115/$ - see front matter © 2007 Elsevier B.V. All rights reserved.
doi:10.1016/j.jnucmat.2007.05.051

that there existed the threshold temperature of the formation of a protective and stable oxide layer that depended on types of steels and oxygen concentrations [18,20]. The erosion–corrosion due to detachment of corroded areas was also reported in the loop test of liquid LBE [13,25]. It was reported recently that the temperature, oxygen concentration, flow velocity, steel composition and thermal gradient play important roles in the corrosion [6–27]. However, we cannot attain to definite and quantitative conclusions because the results obtained are still scarce and scattered.

With the aim of predicting corrosion at each place of plant systems using LBE, corrosion models in simple non-isothermal LBE flow loops have been developed [28–30]. The corrosion models are mainly composed of dissolution of steel elements at high temperature parts, mass transfer due to flow of LBE and precipitation at low temperature parts. It is necessary to obtain correct experimental data for the effects of temperature, oxygen concentration, flow velocity and steel composition on corrosion in LBE in order to develop the corrosion model.

Static tests in pots and loop tests were conducted to estimate the corrosion. The former is mainly conducted to understand basic corrosion mechanism and make screening of materials. The latter is conducted to study effects of flow velocity and mass transfer from high temperature parts to low temperature parts. Although corrosion in LBE depends on temperature, oxygen concentration, flow velocity, thermal gradient, etc., their dependency has not been fully understood. This paper summarizes results of static corrosion tests conducted under low oxygen concentration conditions while results obtained under high oxygen concentrations have already been reported elsewhere [23,24].

The purpose of the present study is to elucidate corrosion behavior (dissolution of steel elements, penetration of Pb and Bi, oxidation, grain boundary corrosion etc.) of various steels in LBE at low oxygen concentrations. We can get knowledge on types of corrosion, corrosion depth and types of corrosion films in LBE with low oxygen concentrations from the study.

2. Experimental

2.1. Materials and specimens

Table 1 shows chemical compositions of test materials. The SX steel is an alloy developed for use in a sulfuric acid environment and the characteristic of the steel is high Si content. Since it was reported that Si addition to steels improves corrosion resistance in liquid LBE [2,3,15,23], the corrosion test for the SX steel was conducted. Corrosion specimens are rectangular plates with the size of 15 mm × 30 mm × 2 mm, and a hole of 7.2 mm diameter is made for installation at the upper part of the specimen. The surface of corrosion specimens is polished using emery papers up to #600.

2.2. Corrosion test apparatus and procedure

Fig. 1 shows a schematic diagram of a corrosion test apparatus in liquid LBE and specimen arrangement. Components contacting liquid LBE were made of quartz. As received eutectic Pb–Bi (45Pb–55 Bi) of 7 kg was used in each test of the present experiment. The chemical compositions were 55.60 Bi–0.0009Sb–0.0002Cu–0.0001Zn–0.0005Fe–0.0007As–0.0005Cd–0.0001Sn–Bal.Pb (wt%). Corrosion tests were conducted at 450 °C and 550 °C for 3000 h. The temperature was measured using a thermocouple at the same depth as the specimen location. Nine specimens of materials listed in Table 1 were exposed to the liquid LBE in the pot. The ratio of the specimen surface area to the liquid LBE volume was about 100 cm^2/l.

The LBE was melted with Ar cover gas with purity of 99.9999%. Specimens were immersed and Ar–4%H_2 gas was bubbled in the liquid LBE after the temperature of liquid LBE arrived at the corrosion test temperature. Inner diameter of the quartz tube for bubbling was 2 mm. The flow rate of Ar–4%H_2 gas was 100 cm^3/min during the first two days and about 20 cm^3/min afterwards until the end of the test on the basis of results described later in the measurement of oxygen concentrations during Ar–4%H_2 gas bubbling in LBE. Specimen arrangement is shown in

Table 1
Chemical compositions of materials tested in the static corrosion experiment (wt%)

	C	Si	Mn	Cr	Ni	Mo	Fe	V	N	W	Ti	Al	Cu
F82H[a]	0.095	0.10	0.01	7.72	<0.02	<0.01	Bal.	0.18	0.010	1.95	0.005	<0.001	–
Mod.9Cr–1Mo steel[a]	0.10	0.30	0.40	8.41	0.06	0.88	Bal.	0.20	0.047	<0.0005	<0.01	0.033	–
14Cr–16Ni–2Mo(JPCA)[b]	0.058	0.50	1.54	14.14	15.87	2.29	Bal.	0.03	0.003	0.010	0.22	0.012	–
410SS[a]	0.067	0.31	0.80	12.21	0.12	0.02	Bal.	0.07	0.013	–	<0.01	0.002	–
430SS[a]	0.080	0.52	0.23	16.24	0.15	0.02	Bal.	0.10	0.024	–	<0.01	0.007	–
2.25Cr–1Mo steel[a]	0.10	0.34	0.44	2.18	0.02	0.92	Bal.	0.01	0.009	–	<0.01	0.002	–
Pure iron	0.002	–	–	–	–	–	Bal.	–	0.001	–	–	–	–
316SS[b]	0.04	0.69	1.22	16.83	10.79	2.06	Bal.	–	–	–	–	–	–
SX[b,c]	0.010	4.80	0.60	17.58	19.08	0.356	Bal.	–	–	–	–	–	2.14

[a] Ferritic/martensitic steels.
[b] Austenitic steels.
[c] Trademark of the Sandvik Corporation.

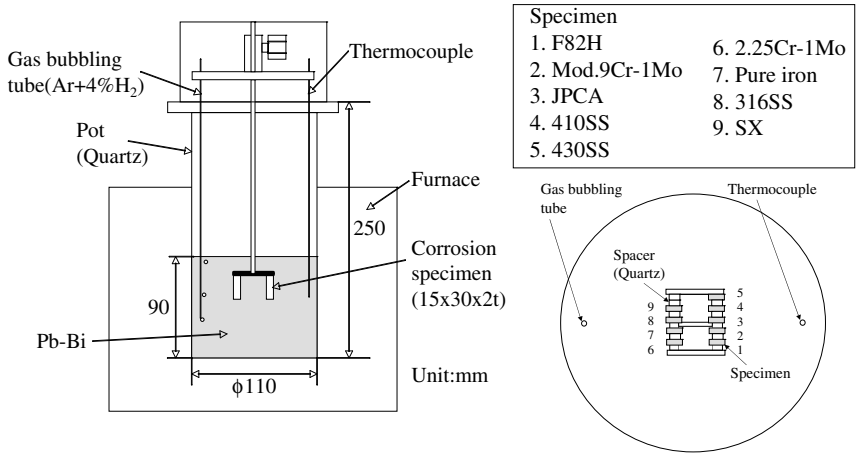

Fig. 1. Schematic diagram of a corrosion test apparatus and specimen arrangement.

Fig. 1. A ring spacer made of quartz was inserted at the upper part of specimens so that specimens did not contact with each other. The gas bubbling tube was located to prevent collision of gas injected in the liquid LBE at specimens. A small quartz container was immersed in the LBE at the same depth as those of specimens to sample the LBE at the start of the test and pulled out at the end of the test.

Test specimens were rinsed in silicone oil at 170 °C after the corrosion tests to remove adherent LBE on the surface of the specimens. However, the LBE could not be removed completely. The cut specimens were plated with copper and molded into resin to protect corrosion films during polishing. Analyses were made using an optical microscope, a scanning electron microscope (SEM) with energy dispersion X-ray (EDX) and a laser microscope.

The corrosion depth was measured using an optical microscope and a SEM. The corrosion depth is the sum of corrosion film thickness, grain boundary corrosion depth, hollow depth, penetration depth of Pb and Bi, and thickness of the formed ferrite layer. The corrosion depth is the average of about 5 measurements obtained at the places where corrosion is deep.

2.3. Oxygen concentration in liquid LBE

An oxygen sensor was made of a cylindrical solid electrolyte, ZrO_2–8 mol%Y_2O_3 with a reference electrode of Pt/air system. The sizes of the normal type oxygen sensor were 15 mm in diameter and 350 mm in length. The oxygen concentration was measured under the condition where Ar–4%H_2 gas was bubbled in liquid LBE using the same corrosion apparatus as that employed in the corrosion test. The oxygen sensor using the solid electrolyte is represented by the following concentration cell:

$$P_{O_{2ref}}//\text{solid electrolyte}//P_{O_2}, \tag{1}$$

where $P_{O_{2ref}}$ and P_{O_2} are the oxygen partial pressures of the reference electrode and of the working electrode in the liquid LBE. The electromotive force, E is given by the Nernst equation:

$$E = \frac{RT}{4F}\ln\frac{P_{O_{2ref}}}{P_{O_2}}, \tag{2}$$

where R is the gas constant, T the temperature in the unit of K and F the Faraday constant. According to Courouau et al. [31], the following equation among E, T and oxygen concentration, C_O in liquid LBE is drawn for oxygen sensor with a reference system of Pt/air when E is lower than that of oxygen-saturation:

$$E = 0.791 - 4.668\times10^{-4}T - 4.309\times10^{-5}T\ln C_O. \tag{3}$$

Fig. 2 shows a time-response of the E values during Ar–4%H_2 gas bubbling. The flow rate of Ar–4%H_2 was the same as described in 2.2. It is found that the E values increased with time and attained constant at each tempera-

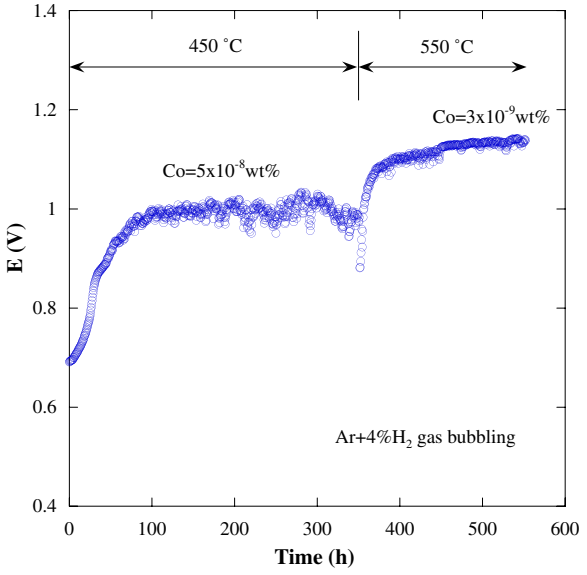

Fig. 2. Electromotive force(E) of oxygen sensor and oxygen concentration in liquid LBE during gas bubbling of Ar–4%H_2.

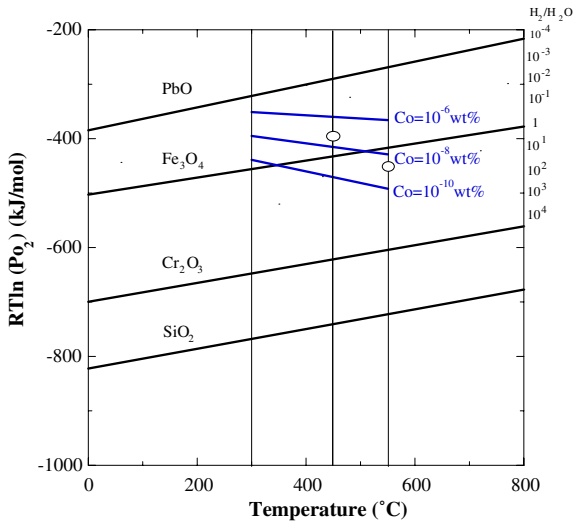

Fig. 3. Oxygen potential diagram of PbO, Fe_3O_4 and other oxides, and oxygen concentrations in liquid LBE as a function of temperature. Experimental conditions are also indicated as circles.

ture during Ar–4%H_2 gas bubbling. Oxygen concentrations in liquid LBE bubbled by Ar–4%H_2 gas were estimated to be 5×10^{-8} wt% at 450 °C and 3×10^{-9} wt% at 550 °C, respectively, as a result of calculation using Eq. (3). Fig. 3 shows the relationship between oxygen potential of oxide formation for Pb, Fe, Cr and Si, and temperature with lines of constant oxygen concentrations in LBE. Open circles indicate the present conditions. The oxygen potential at 450 °C is above that of Fe_3O_4 formation and the oxygen potential at 550 °C is below it. It was expected that Fe_3O_4 was formed at 450 °C and was not at 550 °C.

2.4. Concentrations of Ni, Cr and Fe in LBE after corrosion test

Concentrations of Ni, Cr and Fe in LBE were measured by inductively coupled plasma atomic-emission spectrometry (ICP-AES). Table 2 shows concentrations of Ni, Cr and Fe in LBE before and after the corrosion test and the solubility of each element. The solubilities of Ni, Cr and Fe in LBE, C_{Ni}, C_{Cr} and C_{Fe}, respectively, were calculated using the following equations [1]:

Table 2
Concentrations of Ni, Cr and Fe in LBE (a) before and (b) after corrosion test and solubility

	Temperature (°C)	Concentration (wt%)		Solubility (wt%)
		(a)	(b)	
Ni	450	$<2\times10^{-4}$	$<2\times10^{-4}$	2.31
	550		3.0×10^{-4}	3.21
Cr	450	$<2\times10^{-4}$	$<2\times10^{-4}$	6.72×10^{-4}
	550		$<2\times10^{-4}$	1.62×10^{-3}
Fe	450	$<1\times10^{-4}$	3.0×10^{-3}	1.10×10^{-4}
	550		3.1×10^{-3}	6.01×10^{-4}

$$\log C_{Ni} = 1.53 - 843/T, \quad (4)$$
$$\log C_{Cr} = -0.02 - 2280/T, \quad (5)$$
$$\log C_{Fe} = 2.1 - 4380/T. \quad (6)$$

As shown in Table 2 the Ni solubility in liquid LBE is much higher than the measured concentration. The Ni depletion at the steel surface was observed for austenitic stainless steels as mentioned later. The Cr concentration in LBE is below the detection limit. The Fe concentrations after the corrosion test were five and thirty times as much as the solubility at 550 °C and 450 °C, respectively.

The measured concentrations of Fe in LBE were much higher than the solubility limit after the corrosion test in pots. There might exist oxides including Fe and nuclei or fine grains of Fe crystals in LBE during the corrosion test. No increase in the Fe concentration was recognized in the experiments under the condition of oxygen-saturated LBE where oxides including Fe were formed at the surface of specimens at 450 °C and 550 °C [23,24]. It is probable that the measured high Fe concentration is due to the existence of nuclei or fine grains of Fe crystals. In particular, it is considered that nuclei or fine grains of Fe crystals exist at the surface of liquid LBE when the surface temperature of liquid LBE is lower than the inside temperature in a pot corrosion test with cover gas.

Fig. 4 shows a temperature profile near the surface of the liquid LBE. The surface temperature of liquid LBE is 420 °C in the corrosion test at 450 °C. The surface temperature is 525 °C in the corrosion test at 550 °C. The Fe dissolved at 550 °C in liquid LBE becomes over-saturated near the surface of 525 °C and produces nuclei or fine grains of Fe crystals. The LBE near the surface was also sampled in a quartz container when it was pulled out from liquid LBE. The corrosion proceeded as a result of mass transfer and formation of nuclei or fine grains of Fe

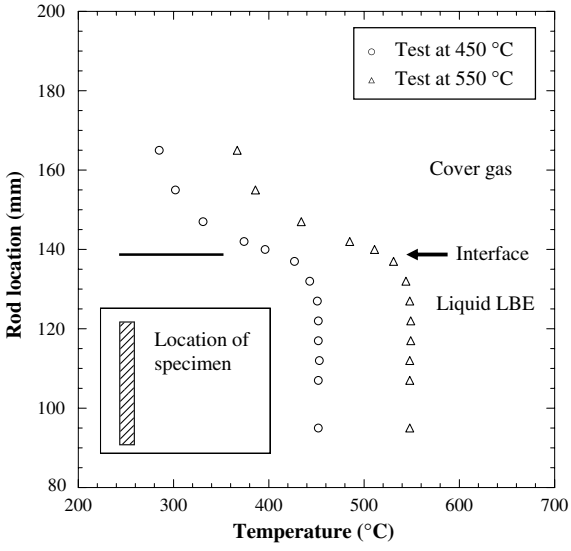

Fig. 4. Temperature profile near the interface between cover gas and liquid LBE in corrosion tests.

crystals near the surface even after the Fe concentration has reached the solubility at the test temperature. For this reason more severe corrosion might occur in the present test than that in an isothermal test.

3. Results and discussion

3.1. Distinctive feature of corrosion based on observation using an optical microscope

Figs. 5 and 6 show optical micrographs of the cross-sections of specimens after corrosion tests at 450 °C and 550 °C, respectively. Observation was performed for transverse and longitudinal sections of each specimen. The following parts are recognized in most micrographs of Fig. 5: the top black part is a resin, the second white one Cu plating, the third grey one corroded layers described in detail later and the lower white one a metal matrix.

Significant corrosion was not found for F82H, Mod.9Cr–1Mo steel, 410SS, 430SS and SX as shown in Fig. 5 (a), (b), (d), (e) and (i). A grey layer of about 40 μm in thickness is formed between an indistinct corrosion film and a white metal matrix of 316SS of Fig. 5(h). The grey layer is a ferrite layer formed in the austenitic stainless steel. Dissolution of Ni and Cr occurs in a ferrite layer. A thin ferrite layer is also found in JPCA of Fig. 5(c). Rough surfaces are recognized for 2.25Cr–1Mo steel and pure iron in Fig. 5(f) and (g), respectively.

Severe corrosion attack was observed at 550 °C. A corroded layer where liquid LBE penetrated from the surface is formed in F82H, Mod.9Cr–1Mo steel and 410SS of Fig. 6(a), (b) and (d), respectively. Corrosion is not so severe in 430SS containing 16 wt%Cr as shown in Fig. 6(e). A ferrite layer is formed at the whole surface in JPCA and 316SS of Fig. 6(c) and (h), respectively. In particular, a ferrite layer of 350 μm in depth is formed in 316SS. The penetration of Pb and Bi along grain boundaries and large holes made by detachment of grains are found in 2.25Cr–1Mo steel of Fig. 6(f). Large hollows are recognized in pure iron of Fig. 6(g). Although correct values of weight change could not be obtained by rinse using silicone oil, large weight loss of 500 g/m^2 was recognized for the pure iron specimen after the corrosion test at 550 °C for 3000 h. Local ferritization is observed in SX of Fig. 6(i).

3.2. Corrosion behaviors of various steels

3.2.1. Ferritic/martensitic steels (F82H, Mod.9Cr–1Mo, 410SS, 430SS, 2.25Cr–1Mo)

As an example of the corrosion film, line analysis of Mod.9Cr–1Mo steel exposed to LBE at 450 °C using EDX is shown in Fig. 7. Adherent Pb–Bi is left on the thin corrosion film. There are clear peaks of O and Cr, and some content of Fe seems to exist. The corrosion film is considered to be a Fe–Cr spinel oxide. The formation of Fe_3O_4 was possible under the condition of an oxygen concentration of 5×10^{-8} wt% in liquid LBE at 450 °C. However, a single-layer oxide film is found instead of double-layer oxide films. In the corrosion tests under the con-

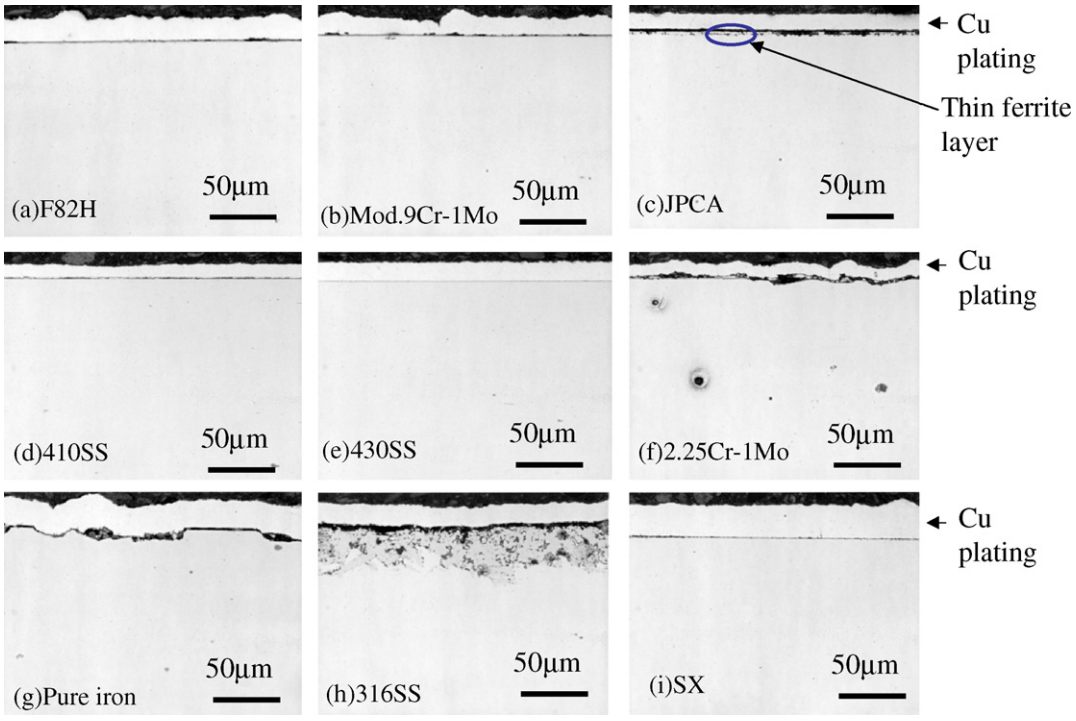

Fig. 5. Optical micrographs of cross-sections of specimens after corrosion test in liquid LBE with an oxygen concentration of 5×10^{-8} wt % at 450 °C for 3000 h.

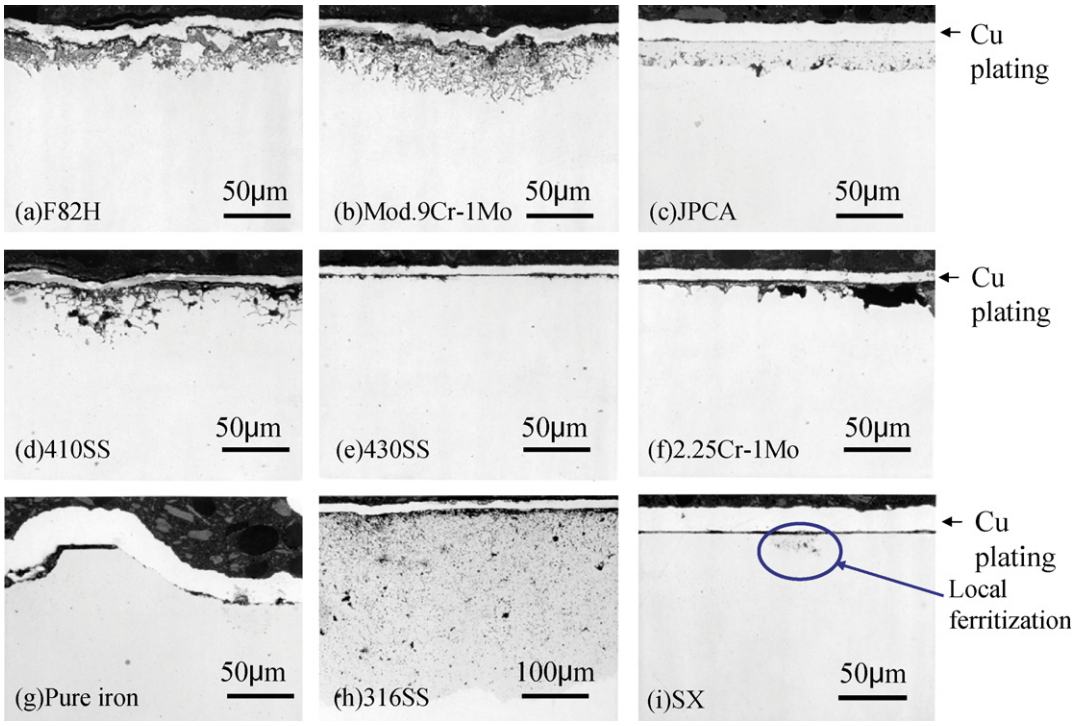

Fig. 6. Optical micrographs of cross-sections of specimens after corrosion test in liquid LBE with an oxygen concentration of 3×10^{-9} wt % at 550 °C for 3000 h.

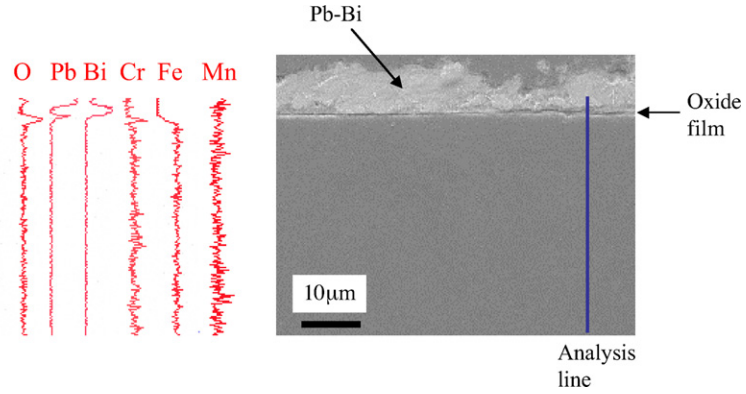

Fig. 7. Line analysis of the cross-section of Mod.9Cr–1Mo steel after corrosion test in liquid LBE with an oxygen concentration of 5×10^{-8} wt% at 450 °C for 3000 h.

dition of high oxygen concentrations in liquid LBE the double-layer oxide films composed of a porous Fe_3O_4 outer layer and a Cr-rich spinel inner layer were often observed [7,16,23,24,26]. Corrosion attack by liquid LBE was not so severe at 450 °C under the conditions of high and low oxygen concentrations. Therefore, it was considered that the formed Fe–Cr spinel oxide contributed to protect the material at 450 °C.

Fig. 8 shows the result of element mapping for the cross-section of F82H after the corrosion test at 550 °C. The complicated shape of the interface of F82H is made by dissolution of elements and Pb–Bi penetration. Line analysis of the cross-section of F82H made using EDX is shown in Fig. 9. An oxide film exists around the area subjected to dissolution and Pb–Bi penetration. The corrosion film is considered to be Mn–Cr spinel oxide. The oxide film containing Mn was also observed in Mod.9Cr–1Mo steel. The oxide film such as Mn–Cr spinel oxide failed to prevent dissolution and Pb–Bi penetration.

Fig. 10 shows a typical example of grain boundary corrosion observed in 2.25Cr–1Mo steel. Liquid LBE penetrates along grain boundaries and grains drop out. The area is seen in the upper photo of Fig. 10. Although oxide films are found at the surface and grain boundaries of 2.25Cr–1Mo steel, they fail to prevent penetration of liquid LBE. Fig. 11 shows the result of element mapping for the cross-section of 410SS including 12 wt%Cr after the corrosion test at 550 °C. Penetration of Pb and Bi is

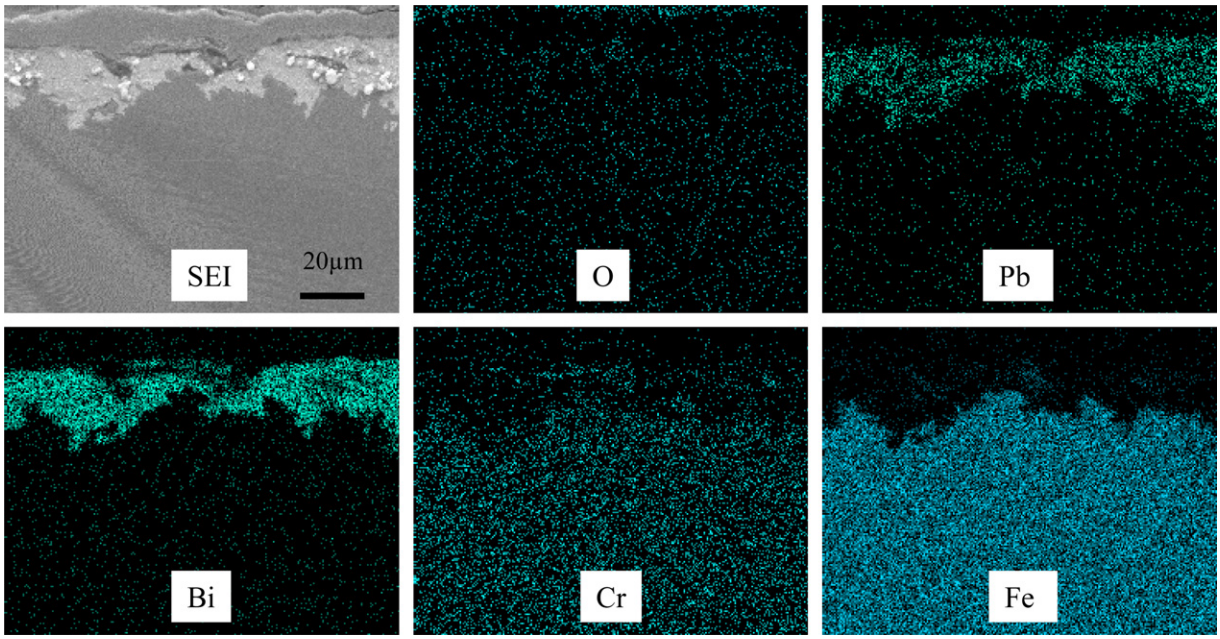

Fig. 8. EDX analysis of the cross-section of F82H after corrosion test in liquid LBE with an oxygen concentration of 3×10^{-9} wt % at 550 °C for 3000 h.

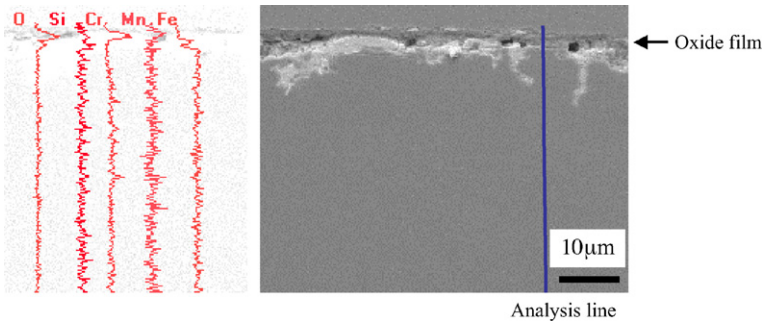

Fig. 9. Line analysis of the cross-section of F82H after corrosion test in liquid LBE with an oxygen concentration of 3×10^{-9} wt% at 550 °C for 3000 h.

also recognized along grain boundaries of 410SS. The grain boundary corrosion under an oxide film is remarkable in liquid LBE with low oxygen concentrations.

In the previous corrosion test at 450 °C under the condition of oxygen-saturated LBE, double-layer oxide films with outer Fe_3O_4 and inner Fe–Cr spinel oxide were often found in ferritic/martensitic steels [23,24]. The outer Fe_3O_4 layer was porous and liquid LBE penetrated into the outer layer. This tendency was accelerated at 550 °C. It had been considered that the protective function was not caused by Fe_3O_4 film under the condition of controlled oxygen concentration within the range between PbO formation and Fe_3O_4 formation. In some papers [16,19,22], it was pointed out that the inner Fe–Cr spinel oxide layer in duplex oxide layers most possibly possessed corrosion resistance under the condition of an oxygen concentration of 10^{-6} wt% or oxygen-saturation. Although there was possibility of Fe–Cr spinel formation at 550 °C in the present experiment, the Mn–Cr spinel oxide formed instead of the Fe–Cr spinel showed inferior corrosion resistance. When the oxygen concentration decreased in liquid LBE, the formed oxide often changed from Fe_3O_4 and Fe–Cr spinel to Mn–Cr spinel oxide which had poor corrosion resistance.

3.2.2. Pure iron

Dissolution of Fe into liquid LBE most possibly occurred if the oxygen concentration was too low to form the oxide film. Since the formation of Fe_3O_4 is not expected under the condition of an oxygen concentration of 3×10^{-9} wt% at 550 °C, Fe atoms can dissolve directly into liquid LBE from the metallic surface. However, the rough surface was also found on pure iron at 450 °C in spite of predicting Fe_3O_4 formation.

Fig. 12 shows 3-dimension images taken by a laser microscope for the surface of pure iron specimens after the corrosion tests. It is found that dissolution of Fe occurred at both temperatures in liquid LBE with the low oxygen concentrations. Dissolution of Fe occurred initially at grain boundaries and crystal planes that were easy to dissolve. When the crystal planes that were difficult to

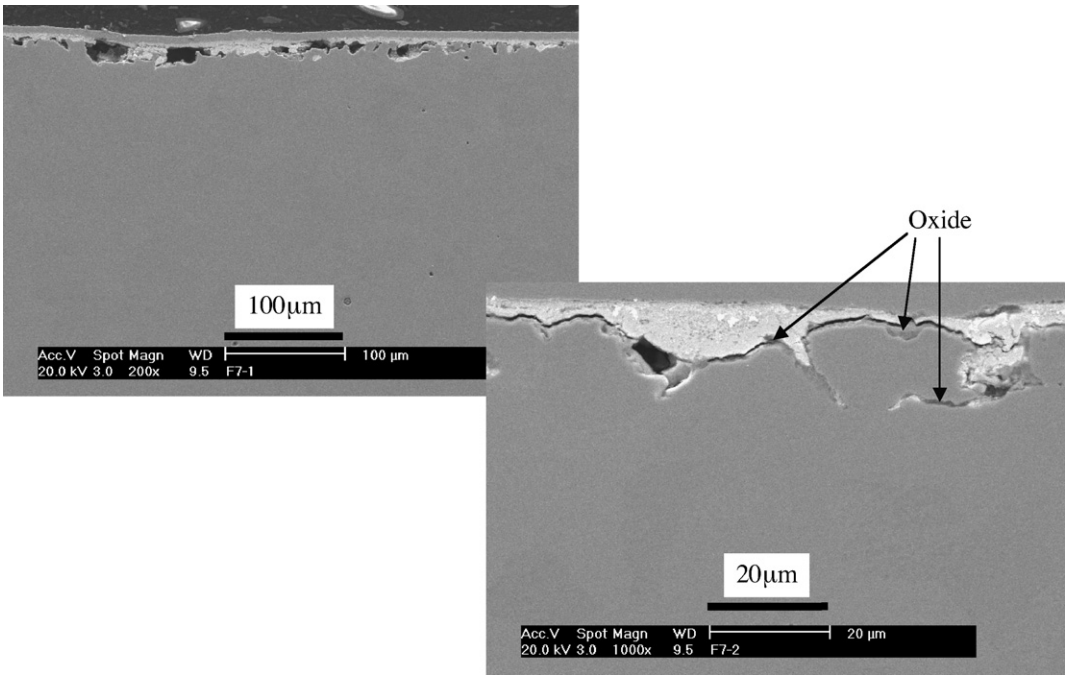

Fig. 10. SEM images of the cross-section of 2.25Cr–1Mo steel after corrosion test in liquid LBE with an oxygen concentration of 3×10^{-9} wt% at 550 °C for 3000 h.

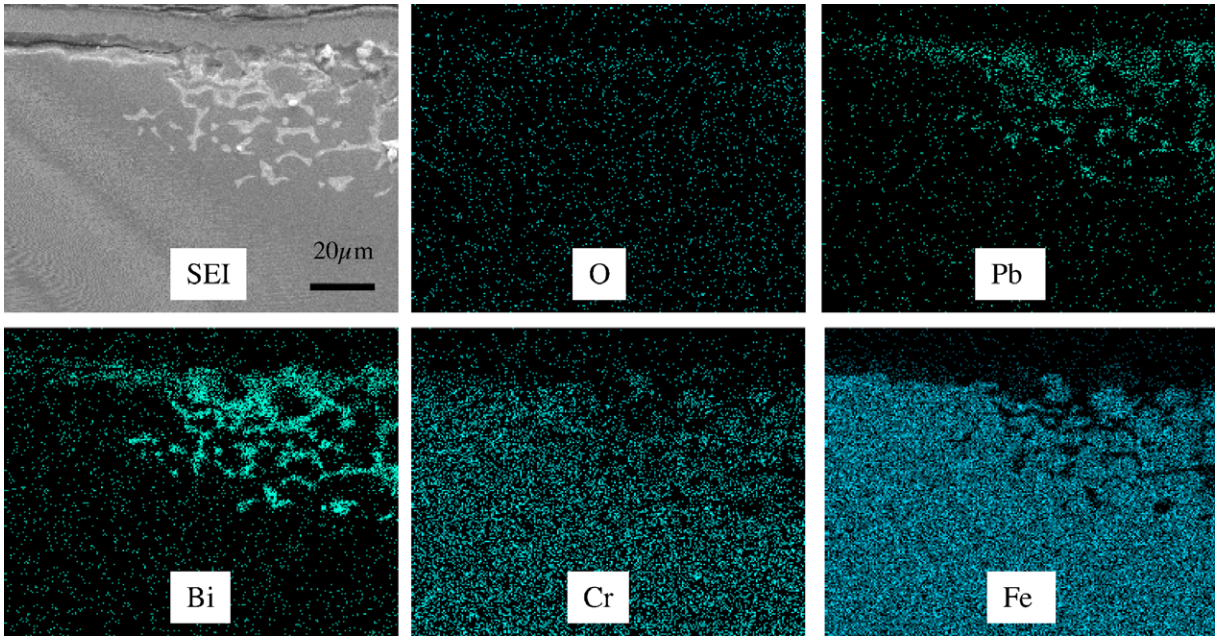

Fig. 11. EDX analysis of the cross-section of 410SS after corrosion test in liquid LBE with an oxygen concentration of 3×10^{-9} wt% at 550 °C for 3000 h.

dissolve existed at the surface, the planes were left and dissolution at grain boundaries proceeded. Fresh planes which appeared by dissolution at grain boundaries produced new sites for the Fe dissolution. This process created the surface configuration shown in Fig. 12. The surface configuration shown in Fig. 12(a) is the middle stage of dissolution, and that at 550 °C in Fig. 12(b) is the stage where dissolution corrosion proceeded to deep level.

There was possibility of Fe_3O_4 formation in the corrosion test at 450 °C. Fig. 13 shows a line analysis of the cross-section of pure iron after the corrosion test in liquid LBE at 450 °C. It is found that the corrosion film is an Fe-oxide from the existence of O and Fe. Dissolution of Fe occurred actually from pure iron at 450 °C even if Fe-oxide is formed. The Fe_3O_4 film formed under the condition of low oxygen concentrations did not have sufficient

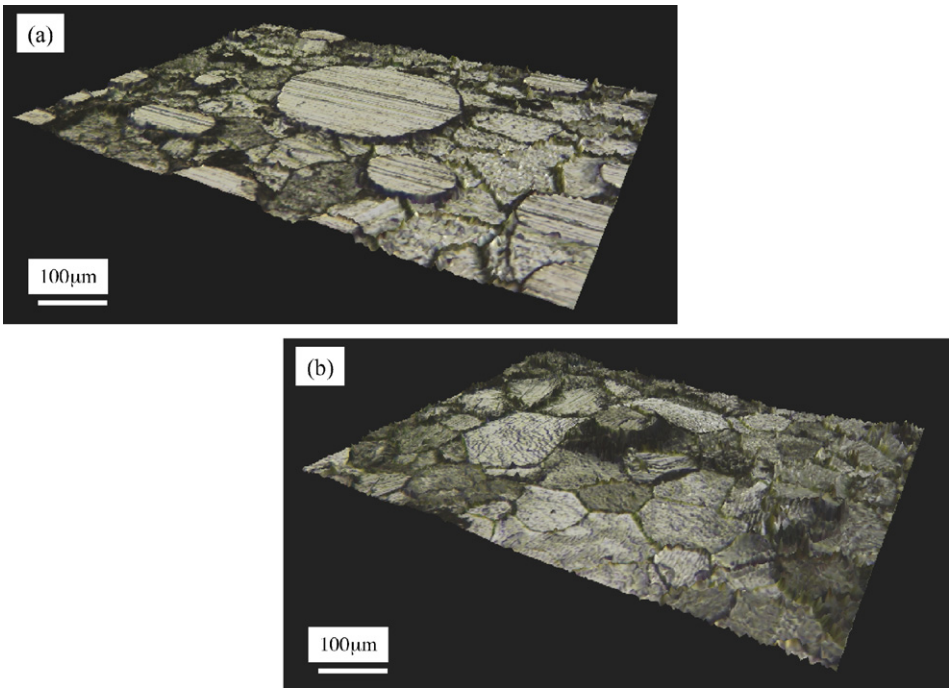

Fig. 12. 3-Dimension images taken by a laser microscope for the surfaces of pure iron specimens after: (a) corrosion test in liquid LBE with an oxygen concentration of 5×10^{-8} wt% at 450 °C for 3000 h and (b) corrosion test in liquid LBE with an oxygen concentration of 3×10^{-9} wt% at 550 °C for 3000 h.

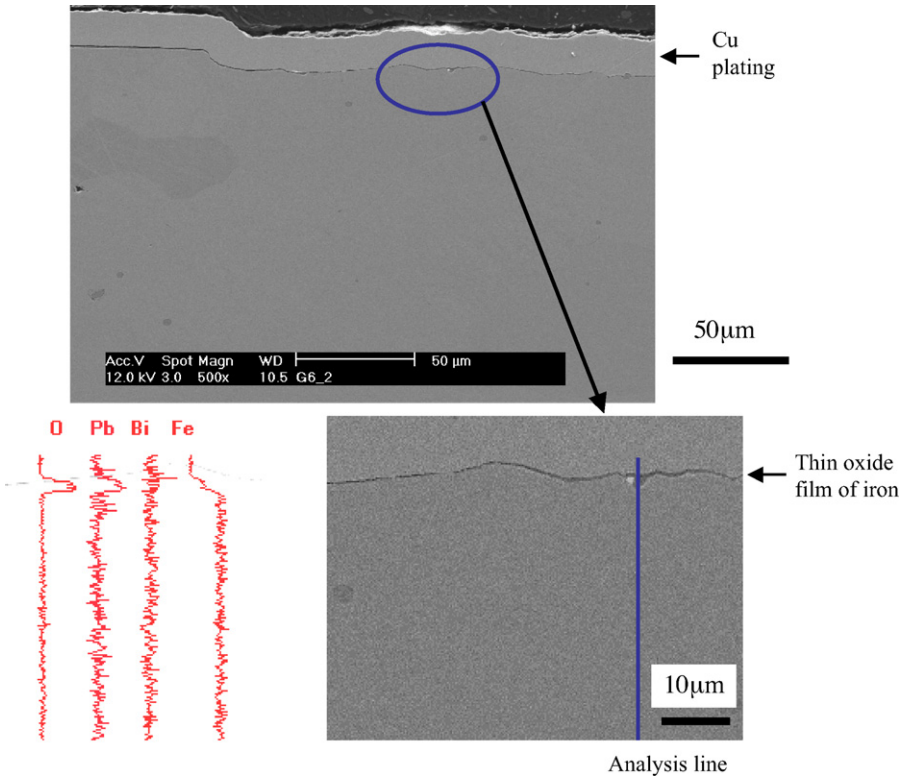

Fig. 13. SEM image and line analysis of the cross-section of pure iron after corrosion test in liquid LBE with an oxygen concentration of 5×10^{-8} wt% at 450 °C for 3000 h.

corrosion resistance. Similar conclusions will be drawn at 550 °C or higher temperatures. The thin Fe_3O_4 film formed under the condition of slightly higher oxygen concentration than that of Fe_3O_4 formation had no prevention of Fe dis-

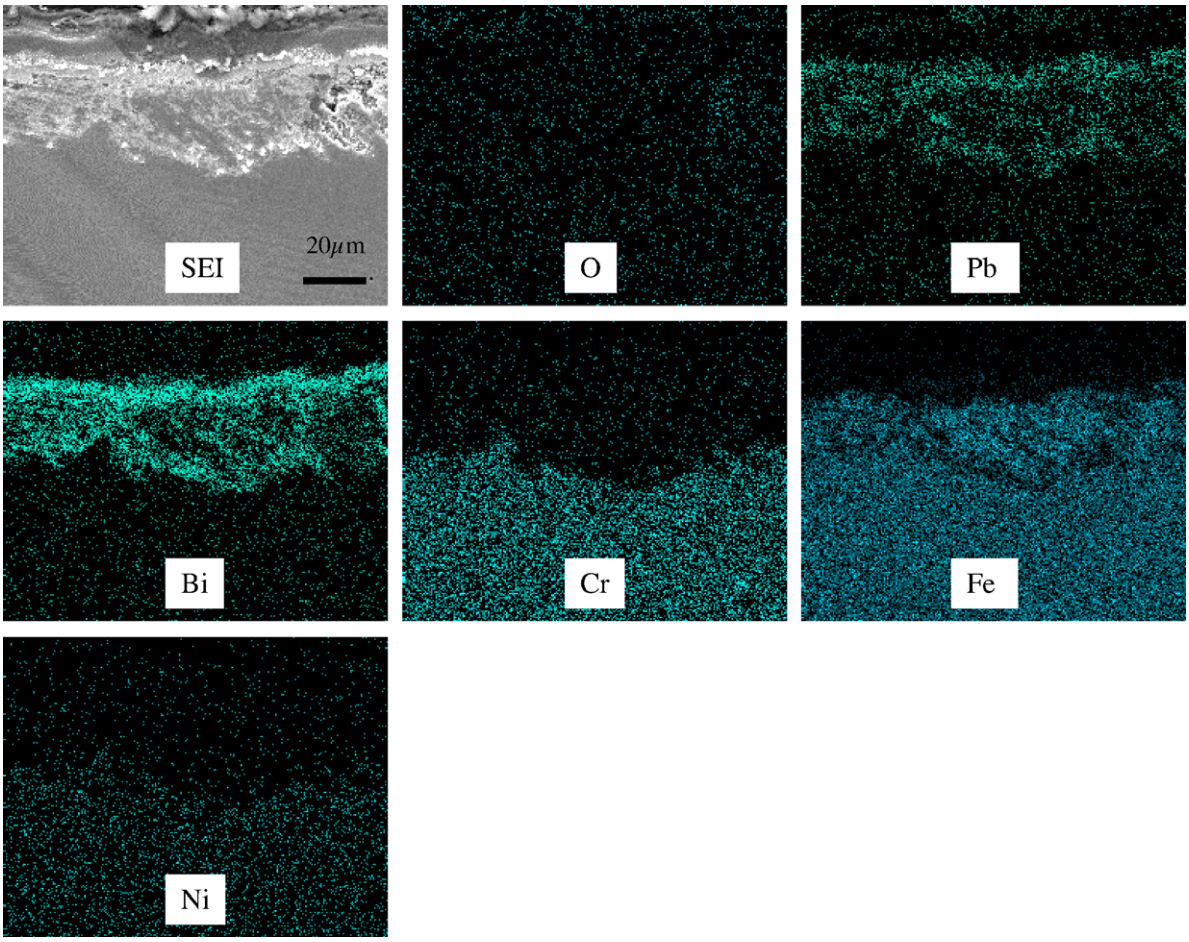

Fig. 14. EDX analysis of the cross-section of 316SS after corrosion test in liquid LBE with an oxygen concentration of 5×10^{-8} wt% at 450 °C for 3000 h.

solution. This result may be explained by high diffusion rate of cation in the oxide film with many defects.

3.2.3. Austenitic stainless steels(316SS, JPCA)

Fig. 14 shows the result of EDX analysis of the cross-section of 316SS after the corrosion test at 450 °C. A ferrite layer was formed by dissolution of Ni and Cr. Pb and Bi penetrate the ferrite layer. This is special feature of corrosion of austenitic stainless steels [9,11,15,17,23]. Fig. 15 shows the result of line analyses of cross-sections of 316SS after the corrosion tests. The oxide formed at 450 °C contained Mn, Si and some Fe. The oxide containing Mn, Cr and some Si was formed at 550 °C. Ferritization proceeded under the oxide films at both temperatures. Ni dissolution and oxide formation occur simultaneously and the resultant oxide film including many defects may have poor protectiveness.

It is considered that the aggressiveness of corrosion depends on not only temperature but also oxygen concentration in corrosion of austenitic stainless steels in liquid LBE even under conditions where some oxide is formed. It has been reported that ferritization of 316SS or 316 L SS occurred at 550 °C under the condition of oxygen-saturated LBE [9,23]. According to Mueller et al. [11,16] the phenomenon for 316L SS did not occur under the condition of an oxygen concentration of 10^{-6} wt%. Ferritization for 316SS and JPCA occurred at 550 °C and did not occur at 450 °C under the condition of oxygen-saturated LBE in the previous experiment [15,23] using the same apparatus and materials as those in the present experiment. On the other hand, ferritization occurred for both steels at 450 °C under the condition of an oxygen concentration of 5×10^{-8} wt% where Fe_3O_4 could be formed.

Penetration of Pb and Bi occurred not only at grain boundaries but also within grains in austenitic stainless steels, 316SS and JPCA in the present experiment. It is considered that Pb and Bi penetrated into cavities formed by the selective dissolution and diffusion of Ni and Cr within grains. Penetration of Pb and Bi is often observed along grain boundaries in ferritic/martensitic steels. It is guessed that penetration of Pb and Bi is also fast at grain boundaries in austenitic stainless steels. The erosion–corrosion process [13,25] has been reported: since Pb and Bi penetrating grain boundaries weaken the bond of grains, the grains are taken away from the surface by the hydrodynamic forces of LBE flow. In a recent paper [25] the erosion–corrosion process was emphasized in the loop test. The specimens were not exposed to the liquid LBE

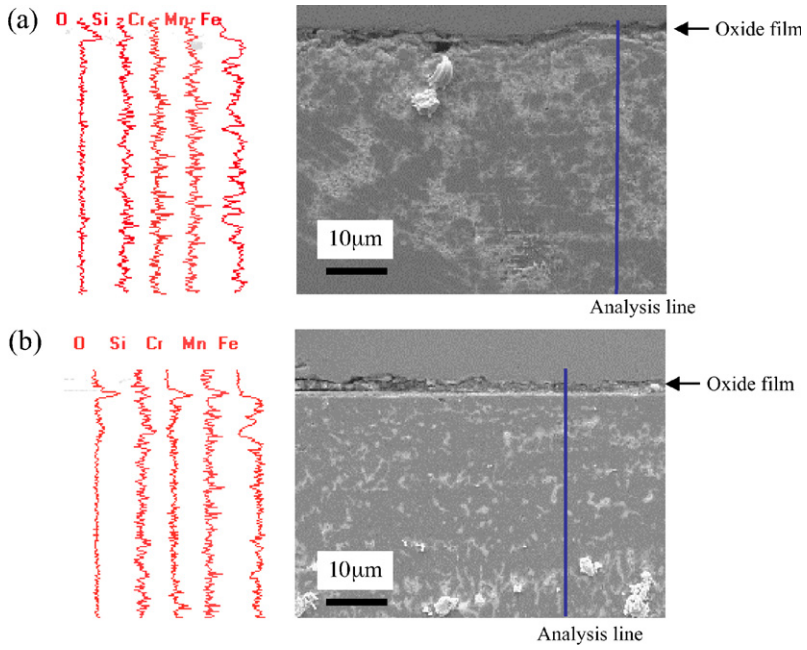

Fig. 15. Line analyses of cross-sections of 316SS after: (a) corrosion test in liquid LBE with an oxygen concentration of 5×10^{-8} wt% at 450 °C for 3000 h and (b) corrosion test in liquid LBE with an oxygen concentration of 3×10^{-9} wt% at 550 °C for 3000 h.

with high flow rates in the present pot test although there was slow flow due to thermal convection and gas bubbling. However, detachment of grains and ferritization were also observed in the present pot test without high flow rate LBE. This suggests the importance of corrosion as the cause of erosion–corrosion observed in the loop test.

3.2.4. Austenitic stainless steel(SX)

Ferritization occurs locally at 550 °C in austenitic stainless steel containing 5 wt%Si, SX as shown in Fig. 6 although it is not found at 450 °C. Ni dissolution and Pb–Bi penetration were partially observed under the condition of an oxygen concentration of 3×10^{-9} wt% in liquid Pb–Bi at 550 °C while a thin and uniform corrosion film was formed without Pb–Bi penetration at the most part of SX. Fig. 16 indicates a SEM image and a line analysis of the area with a thin and uniform corrosion film. Pb–Bi penetration was not observed. Peaks of O, Si and Cr are found on the thin film. On the other hand, the area with Pb–Bi penetration (white dots) was recognized as is shown in Fig. 17. The depth of Pb–Bi penetration was about 25 μm. The oxide film is thicker than that shown in Fig. 16 and peaks of O, Si, Cr and Mn are found on it. Pb and Bi also exist in the oxide film. Since Mn is apt to dissolve into liquid LBE [32], it is anticipated that a complex oxide including Mn does not have sufficient protectiveness and bring the penetration of Pb and Bi. This fact is recognized for not only SX but also ferritic/martensitic steels and 316SS. It is suggested that Mn oxidized in low oxygen concentrations produced an oxide film with inferior corrosion resistance in liquid LBE.

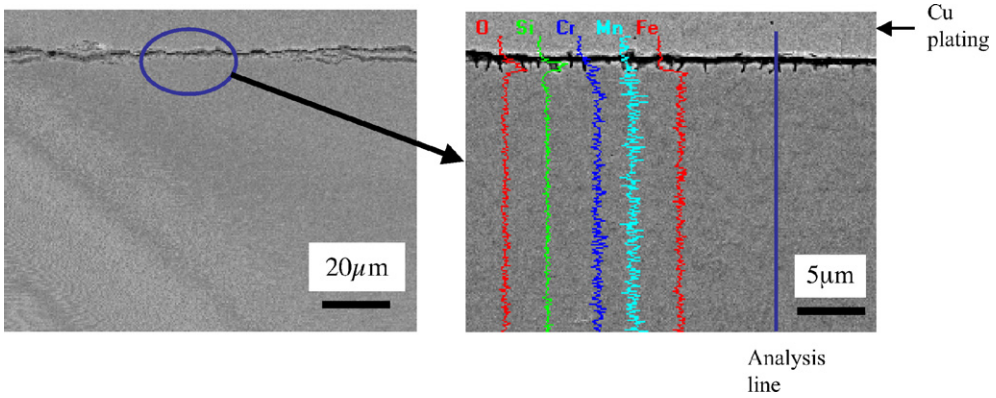

Fig. 16. SEM image and line analysis of the thin film part of the cross-section of SX after corrosion test in liquid LBE with an oxygen concentration of 3×10^{-9} wt% at 550 °C for 3000 h.

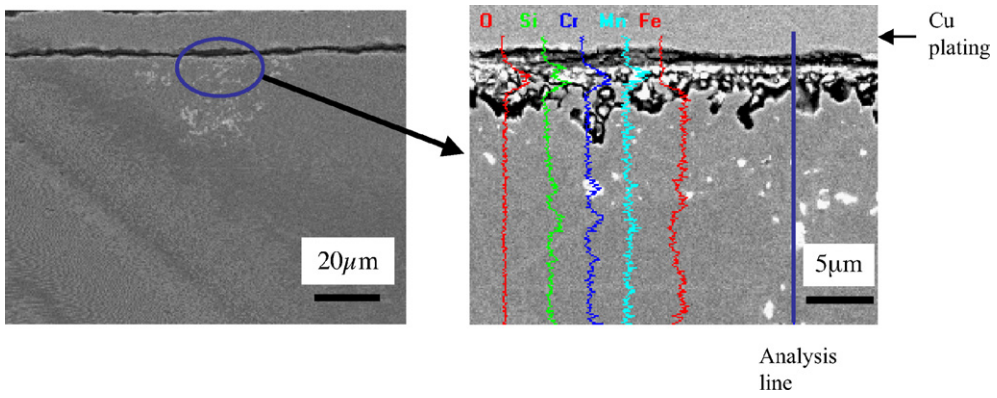

Fig. 17. SEM image and line analysis of the thick film part of the cross-section of SX after corrosion test in liquid LBE with an oxygen concentration of 3×10^{-9} wt% at 550 °C for 3000 h.

3.3. Comparison of corrosion rates of materials

Table 3 shows measured corrosion depths for 3000 h and estimated corrosion rates per year for various steels. Distinct multi-layer oxides are not necessarily formed at low oxygen concentrations while they are often observed at high oxygen concentrations [7,12,16,23,24,26]. Corrosion depths of 316SS for 3000 h are 80 μm at 450 °C and 350 μm at 550 °C. Corrosion depths of steels except 316SS are small at 450 °C. Corrosion depths for 3000 h at 550 °C are above 35 μm for F82H, Mod.9Cr–1Mo steel, JPCA, 410SS, 2.25Cr–1Mo steel, pure iron and 316SS. Corrosion resistance of 430SS and SX is good at 550 °C.

The corrosion rate per year (365 days) is calculated from the measured corrosion depth assuming a linear rule. The estimated corrosion rates of various steels are shown in Fig. 18. The following standard for material classification based on corrosion rates is employed here from the viewpoints of general design and operation of plants:

A: corrosion rate < 0.1 mm/y,
B: 0.1 mm/y $\leqq$ corrosion rate < 1 mm/y,
C: 1 mm/y $\leqq$ corrosion rate.

The material classification is shown in Table 3. 316SS with the corrosion rate of 0.23 mm/y at 450 °C is grouped into a category B. The other materials are grouped into a category A at 450 °C. However, it is also necessary to investigate corrosion from the viewpoint of corrosion configuration. The corrosion configuration of pure iron, 2.25Cr–1Mo steel and JPCA was similar to that at 550 °C although their corrosion rates were lower. At 450 °C, dissolution of Fe was recognized in pure iron and grain boundary corrosion was observed in 2.25Cr–1Mo

Table 3
Corrosion rates of various steels in liquid LBE with low oxygen concentrations

Temperature (°C)	Specimen	Corrosion depth for 3000 h (μm)	Corrosion rate per year (mm/y)	Material classification based on corrosion rate
450	F82H	5.7	0.02	A
	Mod.9Cr–1Mo	4.0	0.01	A
	JPCA	4.7	0.01	A
	410SS	3.0	0.01	A
	430SS	1.5	0.004	A
	2.25Cr–1Mo	11	0.03	A
	Pure iron	19	0.06	A
	316SS	80	0.23	B
	SX	1.1	0.003	A
550	F82H	35	0.10	B
	Mod.9Cr-1Mo	50	0.15	B
	JPCA	40	0.12	B
	410SS	50	0.15	B
	430SS	15	0.04	A
	2.25Cr–1Mo	40	0.12	B
	Pure iron	103	0.30	B
	316SS	350	1.02	C
	SX	25	0.07	A

A: corrosion rate<0.1 mm/y.
B: 0.1 mm/y $\leqq$ corrosion rate < 1 mm/y.
C: 1 mm/y $\leqq$ corrosion rate.

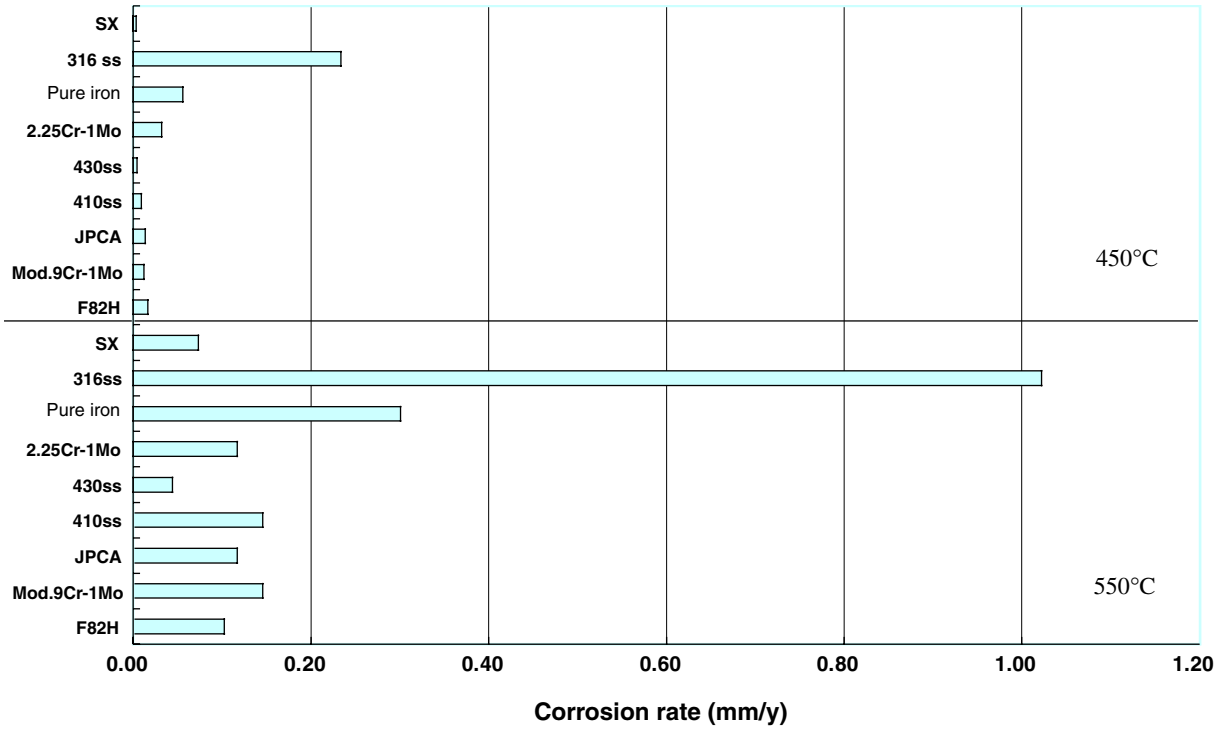

Fig. 18. Estimated corrosion rates per year of various steels in liquid LBE with low oxygen concentrations.

steel. In addition, dissolution of Ni and Cr, and Pb–Bi penetration were found in 316SS and JPCA at 450 °C. 316SS with the corrosion rate of 1.02 mm/y at 550 °C is grouped into a category C. F82H, Mod.9Cr–1Mo steel, JPCA, 410SS, 2.25Cr–1Mo steel and pure iron are grouped into a category B at 550 °C. 430SS and SX are grouped into a category A. According to core design of the ADS plant, the temperature of fuel cladding tubes is likely to be higher than 550 °C. It is expected to be much higher in case of FR with LBE coolant. Core materials in ADS and FR with LBE coolant are used in liquid LBE and under heavy irradiation. 316SS, F82H, Mod.9Cr–1Mo steel and JPCA have comparatively many irradiation data. Under the condition of the low oxygen concentration at 550 °C, their corrosion rates are high.

3.4. Effectiveness of oxide films as a corrosion barrier in liquid LBE

As described in 3.2.2, significant dissolution corrosion was observed at 550 °C in pure iron where Fe_3O_4 was not formed. On the other hand, a thick Fe_3O_4 film was formed on the surface of pure iron in the oxygen-saturated liquid LBE and such significant dissolution of Fe into LBE was not observed [23]. From these two results, the formed Fe_3O_4 shows resistance to dissolution attack. However, a thin Fe_3O_4 film formed on the surface of pure iron under the condition of 450 °C and 5×10^{-8} wt% oxygen failed to prevent dissolution of Fe. These findings suggest that corrosion resistance of the Fe_3O_4 film changes depending on the condition of formation. In addition it has been shown that an outer Fe_3O_4 layer formed on ferritic/martensitic steels in oxygen-saturated liquid LBE is porous and fragile [23].

The Fe–Cr spinel oxide is formed at 450 °C and only slight corrosion occurs in ferritic/martensitic steels except 2.25Cr–1Mo steel. In contrast with this, significant corrosion occurs together with the indication of formation of Mn–Cr spinel oxide at 550 °C. In the results on 316SS and JPCA, oxide films containing Mn are formed and

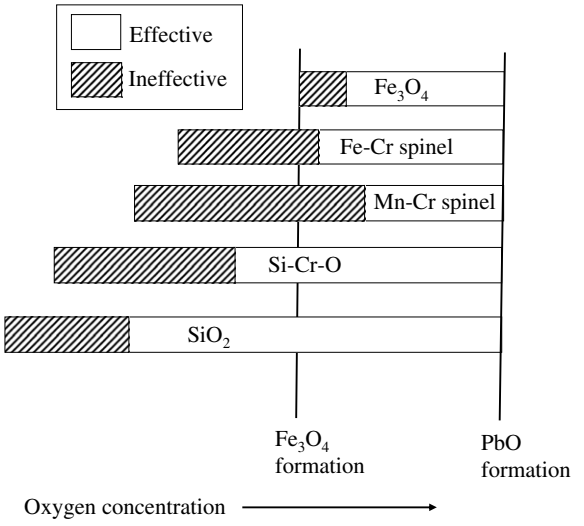

Fig. 19. Schematic diagram about effectiveness of oxide films as a corrosion barrier in liquid LBE. In the active control of oxygen in liquid LBE [3–5], the lower and upper limits are set to the oxygen potential of Fe_3O_4 formation and that of PbO formation, respectively.

dissolution of Ni and Cr, and Pb–Bi penetration occur at both temperatures of 450 °C and 550 °C. An oxide including Si and Cr is formed on SX with Si addition and more protective.

Fig. 19 shows a schematic diagram about the effectiveness of oxide films as a corrosion barrier in liquid LBE. The order of oxides effective to low oxygen concentrations as a corrosion barrier is the following: Si–Cr–O, Fe–Cr spinel oxide, Fe_3O_4 and Mn–Cr spinel oxide. Thermodynamic equilibrium diagram does not necessarily indicate that the oxide formed under the condition is corrosion resistant. It is considered that there are areas where oxides films are ineffective as a corrosion barrier even if they are formed. The oxide film containing Si formed in ferritic/martensitic steels with Si addition was favored at higher temperatures [3]. While formation of pure SiO_2 on steels may be difficult in liquid LBE, oxides containing Si would be protective in LBE with low oxygen concentrations. Corrosion behavior was studied focusing on the analysis of the corrosion film for iron–silicon steel exposed to liquid LBE and three different forms of silicon were found: Si metal, silica and various silicates [27].

4. Conclusions

Corrosion tests in liquid LBE with low oxygen concentrations were performed in pots at 450 °C and 550 °C for 3000 h. Nine steels including pure iron were exposed to liquid LBE with an oxygen concentration of 5×10^{-8} wt% at 450 °C and with an oxygen concentration of 3×10^{-9} wt% at 550 °C under the condition where the temperature of the liquid LBE surface contacting cover gas was 25–30 °C lower than the inside temperature of liquid LBE. The main conclusions are as follows:

(1) Significant corrosion is not observed at 450 °C for ferritic/martensitic steels except 2.25Cr–1Mo steel. At 550 °C, Pb–Bi penetration along grain boundaries and dissolution of elements in steels become severe even for ferritic/martensitic steels. In addition detachment of grains occurs together with the progress of grain boundary corrosion. Although the formation of Mn–Cr spinel oxide is indicated at 550 °C, it fails to prevent the above-mentioned corrosion attack.
(2) Dissolution of Fe into liquid LBE occurs for pure iron in spite of formation of a thin Fe_3O_4 film at 450 °C. The Fe_3O_4 film formed under the condition of the low oxygen concentration does not have sufficient corrosion resistance. Severe dissolution of Fe and hollows are recognized without a Fe_3O_4 film under the condition at 550 °C.
(3) Dissolution of Ni and Cr, and Pb–Bi penetration occur for 316SS and JPCA under the condition at 450 °C. Ferritization due to the selective element dissolution and Pb–Bi penetration are more severe for 316SS and JPCA at 550 °C than at 450 °C. The oxide films formed at 450 °C and 550 °C contain Mn and do not have sufficient corrosion resistance. Ferritization and Pb–Bi penetration occur locally at 550 °C for SX including 5 wt% Si although they are not observed at 450 °C.
(4) Corrosion depths of 316SS for 3000 h are 80 μm at 450 °C and 350 μm at 550 °C. Corrosion depths of steels except 316SS are small at 450 °C. Corrosion depths for 3000 h at 550 °C are above 35 μm for F82H, Mod.9Cr–1Mo steel, JPCA, 410SS, 2.25Cr–1Mo steel, pure iron and 316SS. Corrosion resistance of 430SS and SX is good at 550 °C.

Acknowledgement

The authors are grateful to Dr H. Oigawa for his encouragement of the present study.

References

[1] B.F. Gromov, Y.I. Orlov, P.N. Martynov and V.A. Gulevsky, in: Proceedings of Heavy Liquid Metal Coolants in Nuclear Technology, HLMC'98, October 5–9, 1998, Obninsk, Russia, 1999, p. 87.
[2] I.V. Gorynin, G.P. Karzov, V.G. Markov, V.S. Lavrukihin and V.A. Yakovlev, in: Proceedings of Heavy Liquid Metal Coolants in Nuclear Technology, HLMC'98, October 5–9, 1998, Obninsk, Russia, 1999, p. 120.
[3] G.S. Yachmenyov, A.Ye. Rusanov, B.F. Gromov, Yu. S. Belomytsev, N.S. Skvortsov, A.P. Demishonkov, in: Proceedings of Heavy Liquid Metal Coolants in Nuclear Technology, HLMC'98, October 5–9, 1998, Obninsk, Russia, 1999, p. 133.
[4] N. Li, J. Nucl. Mater. 300 (2002) 73.
[5] J.L. Courouau, J.C. Robin, J. Nucl. Mater. 335 (2004) 264.
[6] G. Mueller, G. Schumacher, F. Zimmermann, J. Nucl. Mater. 278 (2000) 85.
[7] F. Barbier, G. Benamati, C. Fazio, A. Rusanov, J. Nucl. Mater. 295 (2001) 149.
[8] F. Barbier, A. Rusanov, J. Nucl. Mater. 296 (2001) 231.
[9] G. Benamati, C. Fazio, H. Piankova, A. Rusanov, J. Nucl. Mater. 301 (2002) 23.
[10] Y. Kurata, M. Futakawa, K. Kikuchi, S. Saito, T. Osugi, J. Nucl. Mater. 301 (2002) 28.
[11] G. Mueller, A. Heinzel, J. Konys, G. Schumacher, A. Weisenburger, F. Zimmermann, V. Engeliko, A. Rusanov, V. Markov, J. Nucl. Mater. 301 (2002) 40.
[12] D. Gomez-Briceno, L. Soler, F.J. Martin, F. Hernandez, J. Nucl. Mater. 303 (2002) 137.
[13] Y. Kurata, K. Kikuchi, M. Futakawa, S. Saito, M. Sasa, JAERI-Conf 2003-001,2003, p. 382.
[14] K. Kikuchi, Y. Kurata, S. Saito, M. Futakawa, T. Sasa, H. Oigawa, E. Wakai, K. Miura, J. Nucl. Mater. 318 (2003) 348.
[15] Y. Kurata, M. Futakawa, J. Nucl. Mater. 325 (2004) 217.
[16] G. Mueller, A. Heinzel, J. Konys, G. Schumacher, A. Weisenburger, F. Zimmermann, V. Engeliko, A. Rusanov, V. Markov, J. Nucl. Mater. 335 (2004) 163.
[17] A. Aiello, M. Azzati, G. Benamati, A. Gessi, B. Long, G. Scaddozzo, J. Nucl. Mater. 335 (2004) 169.
[18] L. Soler, F.J. Martin, F. Hernandez, D. Gomez-Briceno, J. Nucl. Mater. 335 (2004) 174.
[19] F. Gnecco, E. Ricci, C. Bottino, A. Passerone, J. Nucl. Mater. 335 (2004) 185.
[20] F.J. Martin, L. Soler, F. Hernandez, D. Gomez-Briceno, J. Nucl. Mater. 335 (2004) 194.
[21] G. Ilincev, D. Karnik, M. Paulobic, A. Doubkova, J. Nucl. Mater. 335 (2004) 210.

[22] T. Furukawa, G. Mueller, G. Schumacher, A. Weisenburger, A. Heinzel, F. Zimmermann, K. Aoto, J. Nucl. Sci. Technol. 41 (2004) 265.
[23] Y. Kurata, M. Futakawa, S. Saito, J. Nucl. Mater. 343 (2005) 333.
[24] Y. Kurata, M. Futakawa, S. Saito, Japan Atomic Energy Research Institute Report, JAERI-Research 2005-002, 2005.
[25] M. Kondo, M. Takahashi, T. Suzuki, K. Ishikawa, K. Hata, S. Qiu, H. Sekimoto, J. Nucl. Mater. 343 (2005) 349.
[26] J. Zhang, N. Li, Y. Chen, A.E. Rusanov, J. Nucl. Mater. 336 (2005) 1.
[27] A.L. Johnson, E.P. Loewen, T.T. Ho, D. Koury, B. Hosterman, U. Younas, J. Welch, J.W. Farley, J. Nucl. Mater. 350 (2006) 221.
[28] B.X. He, N. Li, M. Mineev, J. Nucl. Mater. 297 (2001) 214.
[29] J. Zhang, N. Li, Oxid. Met. 63 (5/6) (2005) 353.
[30] T. Malkow, H. Steiner, H. Muscher, J. Konys, J. Nucl. Mater. 335 (2004) 199.
[31] J.L. Courouau, P. Trabuc, G. Laplanche, Ph. Deloffre, P. Taraud, M. Ollivier, R. Adriano, S. Trambaud, J. Nucl. Mater. 301 (2002) 53.
[32] J.R. Weeks, Nucl. Eng. Design 15 (1971) 363.